Effect of Screw Axial Vibration on Polymer Melting Process in Single-Screw Extruders

Jinping Qu,* Guansheng Zeng, Yanhong Feng, Gang Jin, Hezhi He, Xianwu Cao

National Engineering Research Center of Novel Equipment for Polymer Processing, The Key Laboratory of Polymer Processing Engineering Ministry of Education, South China University of Technology, Guangzhou 510641, People's Republic of China

Received 21 March 2005; accepted 21 May 2005
DOI 10.1002/app.22293
Published online in Wiley InterScience (www.interscience.wiley.com).

ABSTRACT: A model for investigating the melting process of polymer in a vibration-induced single-screw (VISS) extruder is presented. The key feature of this model is as follows: vibration force field is introduced into the overall course of extrusion by the axial vibration of the screw, and the velocity distribution in the polymer melt behaves strongly nonlinear and time-dependent. To analyze this model, half-open barrel visible experimental method and low-density polyethylene material are adopted to investigate the effect of the vibration parameters on the melting process, which goes into further details of study and research on the melting mechanism, and thus, a novel physical melting model is derived. Combining the conservation equations of mass, movement, energy, and constitutive, analytical expressions of the melting rate, the energy consumption, the length of melting section, and the distribution of solid bed are obtained. This model enables the prediction of the processing and design parameters in the VISS extruders from which the optimum conditions for designing VISS extruder and polymer processing are obtained. The theory is supplemented by a calculation sample and experiment, which shows that the introduction of vibration force field can improve the melting capacity and decrease the power consumption of extruder greatly. © 2006 Wiley Periodicals, Inc. J Appl Polym Sci 100: 3860–3876, 2006

Key words: melt; polymer; extruder; vibration; melting-model

INTRODUCTION

During the past decades, the plasticating extruder has experienced a significant technical development, and a variety of new techniques; skills and equipments have emerged. Among which, vibration-induced single-screw (VISS) extruder is an original creation of Professor Qu JinPing,[1,2] and the key feature of which is the introduction of vibration force field into the whole course of polymer melting. Because of this invention, the melting capacity of the extruder and the product quality have been improved greatly. On the other side, it also helps to reduce the energy consumption and minimize the geometry size of the equipment, which has been proved by scientific experiments and practical works.[1–7]

Theoretical and experimental studies show that,[8–21] development of a representative, theoretical analysis of the melting process in a extruder is an established objective in plastics engineering because of its relevance to a broad class of design and operating problems, such as determination of the melting capacity of the extruder; evaluation of the contribution of the melting zone to the overall characteristics of the screw; prediction of those instabilities and surging phenomena that originate from the melting mechanism; determination of the scale-up rules; and optimization of the performance. Therefore, a lot of experiments and theoretical research works on which had been done by researchers. Among which, Tadmor's Model[8,9] is the pioneer, which is based on the experimental work of Maddock,[10] then successively followed by Street,[11] Vermeulen et al.,[12] and Emdmondson and Fenner.[13] According to their observations, the nonmolten polymer is transported by the action of the screw down the screw channel as a solid bed, and the melting of this takes place at various rates over the interface.

Dekker[14] initiated a visualization experimental program on the melting process in large extruders, and found that the melting mechanism does not conform to the typical Maddock flow pattern characterized by the very thin molten film between the solid bed surface and the barrel, and the dominant melt pool, the width of which increases until the melting is com-

**Present address:* National Engineering Research Center of Novel Equipment for Polymer Processing, South China University of Technology, Guangzhou, China, 510640.
Correspondence to: J. Qu (jpqu@scut.edu.cn).
Contract grant sponsor: National Natural Science Foundation of China; contract grant numbers: 20074010, 10472034, 10590351.
Contract grant sponsor: National Natural Science Equipment Foundation of China; contract grant number: 20027002.

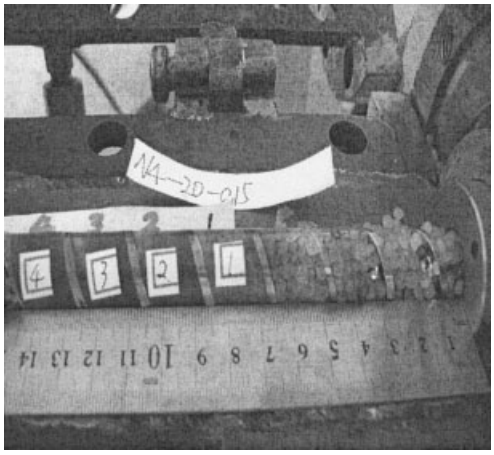

Figure 1 Photo of H-VISS extruder when the barrel is opened.

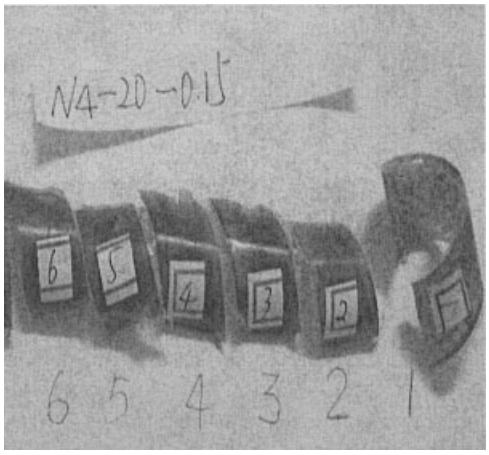

Figure 2 Photo of the material ribbons that comes from the H-VISS extruder (60 rpm), and the frequency is 20 Hz and amplitude is 0.15 mm.

pleted or the solid bed breaks up. In contradistinction to the Maddock mechanism, the melt here seems to accumulate mainly in the melt film itself instead of being predominantly dragged into the melt pool. Finally, the mathematical model based on the Dekker's work has been established by Lindt.[15–18]

Melting in conventional single-screw extruders has been extensively studied and modeled. Nevertheless, with the introduction of vibration force field, the melting mechanism in VISS extruder will be distinct from those in previous theories. Until now, very few published works in this area can be found. The objective of this paper is to study the melting mechanism in the VISS extruder through experimental observation, then establish the melting physical mold and get the approximate analytical expression. Finally, we can verify this through experiments.

Experimental observation

In this section, the half-open barrel visible experimental method and the low-density polyethylene (LDPE) material are used to observe the melting process in VISS extruder, which will be essential for the establishment of physical model.

As shown in Figure 1, the screw in the half-open visualization experimental equipment can vibrate along its axis while it is rotating. There is an additional rapid freezing device installed in the barrel of this equipment. Therefore, it can be cooled down soon after the machine stops. Then, the material ribbon (see Fig. 2) on the melting section can be easily obtained when the barrel is opened, and finally, the frozen polymer ribbon is sectioned. The basic flow pattern was traced back from the various cross sections by locating the boundaries between the originally molten and nonmolten areas; to avoid any ambiguities, small amounts of the solid feedstock were colored. Here, carbon powder was used. A typical result of this procedure as obtained on our 20-mm H-VISS extruder with LDPE is shown in Figure 3.

As shown in Figure 3, during the melting process, the solid bed is located against the trailing interface of the screw flight, the melt pool accumulates along the pushing interface, and a thin melting film separates

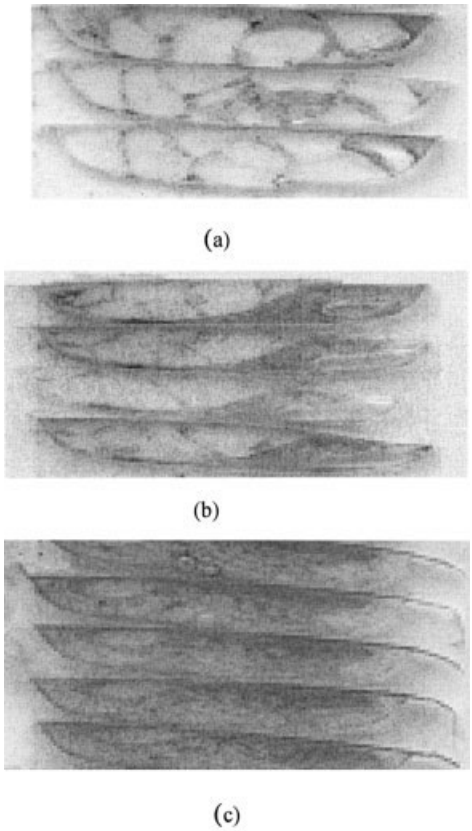

Figure 3 Melting of LDPE in H-VISS extruder (60 rpm), and frequency is 20 Hz and amplitude is 015 mm.

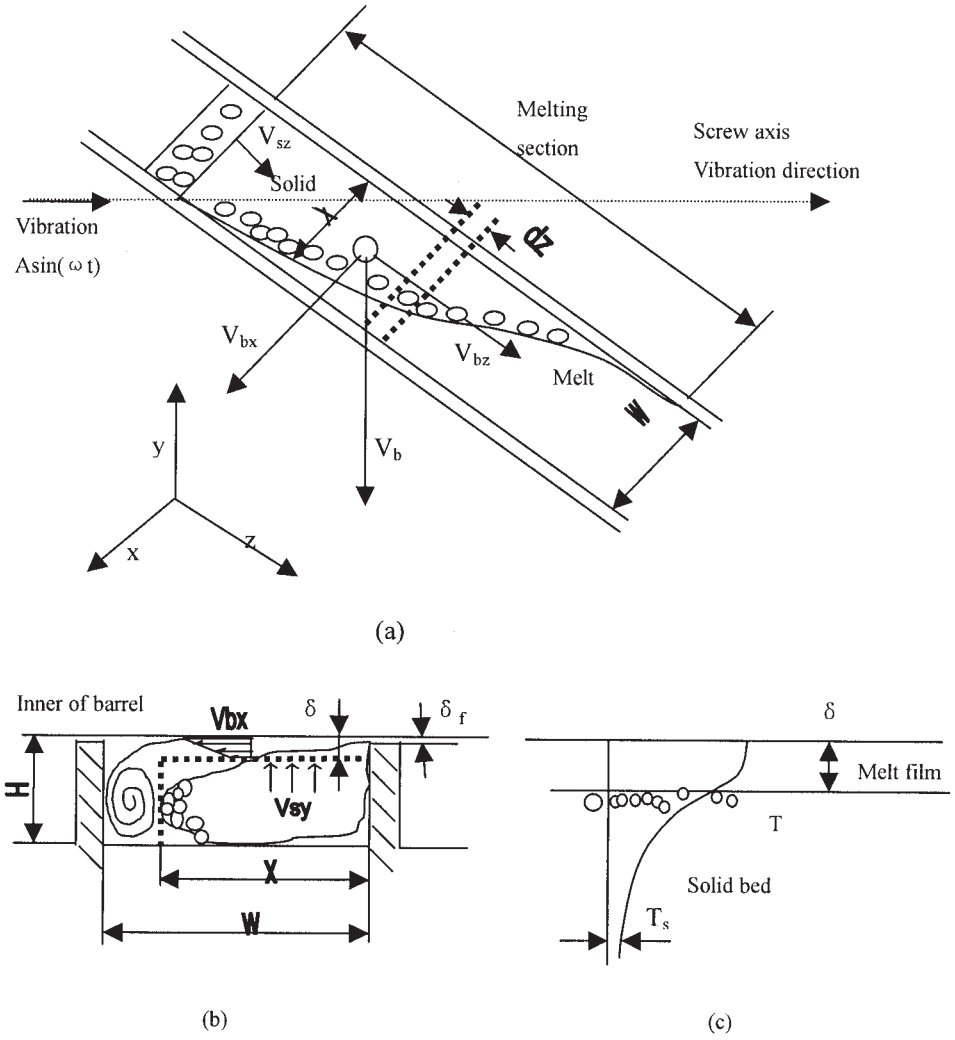

Figure 4 Simplified melting physical model. (a) Illustration of unwrap of the screw channel and coordinate system; (b) illustration of across of the screw channel; and (c) illustration of temperature distribution.

the solid bed and the barrel [Fig. 3(a)]. The back part (add carbon powder in LDPE during experiment) of the slice of material ribbon is the polymer melt, and the light part is the polymer solid. As the melting proceeds, the melt pool gradually grows at the expense of solid bed until eventually the solid bed disappears entirely and the melted polymer material fills the entire section of the screw channel [Fig. 3(b,c)].

MELTING PHYSICAL MODEL

The simplified physical model and coordinate are established, as shown in Figure 4 based on the previous experimental observation. It is in a manner similar to that of Maddock and Tadmor, etc.

Figure 4(a) is the unwrapped figure of the screw channel. As shown in this figure, the head part of the channel is filled with polymer solid, and the end part of the channel is filled with polymer melt. And it is a coexistence of solid and melt in the large part of the middle part of the channel. There is a clear interface, which is separating the solid bed and the melt. We call this part as mix-melting section (or melting section).

Figure 4(b) is the illustration of polymer melting process, and Figure 3(c) is the illustration of temperature distribution along the depth of screw channel.

In VISS extruder, the heat necessary for the material phase conversion is supplied by two sources: first from the hot barrel and second by the viscous dissipation heat. In contradistinction to the conventional extruder (without vibration field), during the course of extrusion, the screw will vibrate along the axis as it rotating. Hence, under the impact of vibration, the melting process behaves strongly dynamic and time-dependent, and the viscosity dissipation heat will play an important role in the melting process of polymer. Because of the screw vibration along its axis, the polymer keeps on abrading, mixing under the impact of

the vibration field while it is under the shear flowing. Meanwhile, it also helps to even the distribution of the temperature of the polymer melt and avoid the partial superheat.

ANALYTICAL MODEL FOR MELTING PROCESS

As stated earlier, the theoretical analysis presented here mainly deals with the mix-melting section of the solid and melt coexistence. We set the point where the thin melt is generated as the starting point. Where, we let $z = 0$, and z means the down-channel direction.

To simplify the deduction, the following assumptions were presumed to hold true:

a. The physical model as shown in Figure 4 applies.
b. Solid bed was homogeneous, continuous and infinite along the down-channel direction.
c. The cross section of solid bed and screw channel were rectangle.
d. The temperature distribution in melt-film is linear.
e. The flow of thermal energy along the screw axes could be neglected.
f. Barrel is mobile, and screw is fixed relatively.
g. The melt of polymer is incompressible.
h. Leakage flow from the flights could be neglected.
i. The pressure grads in melt film can be neglected.

From previous assumptions, the barrel velocity V_b relative to screw is determined by

$$V_b = \pi ND \tag{1}$$

where N is the rotating speed of screw, and D is the inner diameter of barrel. As shown in Figure 4(a), V_b may be split into components V_{bz} and V_{bx} in the down-channel (z) and cross-channel (x) direction, respectively. Herein,

$$V_{bx} = V_b \sin\theta \tag{2}$$

$$V_{bz} = V_b \cos\theta \tag{3}$$

where θ is the helix angle. We can assume the vibration is given as

$$S = A \sin(\omega t) \tag{4}$$

where A is the amplitude, ω is the angle frequency, and t is the time. Hence, the vibration speed of screw Vd will be

$$V_d = \frac{dS}{dt} = A\omega \cos(\omega t) \tag{5}$$

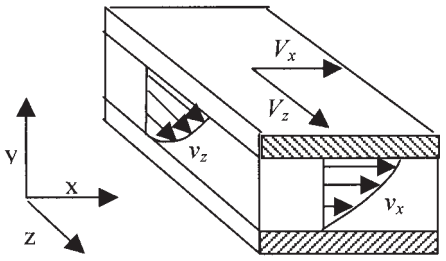

Figure 5 Illustration of three-dimensional model of melt film.

Herewith, we have

$$V_{dz} = V_d \sin\theta \; V_{dx} = V_d \cos\theta \tag{6}$$

Moreover, the solid bed moves at the speed Vsz along down-channel direction (z), and if we also assume that the solid bed is fixed, then the relative velocity of the inner wall of the barrel will be

$$V_x = V_{bx} + V_{dx} \tag{7}$$

$$V_z = V_{bz} + V_{dz} - V_{sz} \tag{8}$$

Therefore, the melt film can be simplified as the three-dimension model (or double-plate model) as shown in Figure 5, where the upper plate denotes the barrel, and it is moving at the speed of V_x and V_z, the other plate denotes the solid bed, and which is fixed. ν_x and ν_z are the velocity distribution in the thickness of melt film along x and z direction, respectively, and y is the direction along the thickness of melt film.

The mass equation of solid bed in z direction

As shown in Figure 4(a), the microunit length dz is used for the present analysis. From the mass conservation equation of solid bed, we have

$$\rho_s V_{sz}(H - \delta)X|_z - \rho_s V_{sz}(H - \delta)X|_{z+\Delta z} = \psi \Delta z \tag{9}$$

where ρ_s is the average density of solid bed, X is the width of solid bed, H is the depth of screw channel, δ is the thickness of melt film, ψ is the melting rate of solid bed per unit length in down-channel direction, z is in down-channel direction, and ΔZ is the finite distance in down-channel direction.

When $\Delta z \to 0$, eq. (9) can be simplified as

$$-\rho_s V_{sz} \frac{d(HX)}{dZ} = \psi \tag{10}$$

Equation (10) demonstrates that the decrease of solid bed is equal to the melting mass of solid bed at melt–solid interface, as well as the mass that was trailed into

the melt pool. Similarly, the melting rate at the melt–solid interface must be equal to the new melt entering the melt film per unit time (VsyρsX), then,

$$\psi = V_{sy}\rho_s X = \rho_m q_x \tag{11}$$

where V_{sy} is the speed of solid bed in y direction (depth of screw channel), ρ_m is the melt density of polymer, and q_x is the flowing rate of polymer melt trailed into melt pool per unit length along down-channel direction.

Energy conservation at melt–solid interface

From assumption (e), y direction is the only way for heat conduction. Moreover, heat convection and radiation can be neglected. Therefore, we have

$$[q_{my}]_{y=0} - [q_{sy}]_{y=0} = \Delta q \tag{12}$$

And from the Fourier law, we obtain

$$q = -k_0 \frac{dT}{dy} \tag{13}$$

Substituting eq. (13) into eq. (14) leads to

$$k_m \left(\frac{dT}{dy}\right)_{y=0} - k_s \left(\frac{dT}{dy}\right)_{y=0} = V_{sy}\rho_s \lambda_0 \tag{14}$$

where q_{my} is the heat conducted from melt film into melt–solid interface, q_{sy} is the heat conducted from melt–solid interface into solid bed, Δq is the heat consumed by the melting of polymer solid, k_0 is the thermal conductivity, k_s is the thermal conductivity of polymer solid, k_m is the thermal conductivity of polymer melt, and λ_0 is the latent heat of fusion of polymer.

Analytical expression of the heat conducted from melt into melt–solid interface

On the basis of previous assumption, the pressure grads inside the melting film as well as the gravity can be neglected. Because of the existence of the vibration field, the inertia term in the momentum equation can not be ignored, then the momentum equation for the melting film along the direction x and y can be simplified as

$$\rho_m \frac{\partial \nu_z}{\partial t} = \frac{\partial \tau_{zy}}{\partial y} \tag{15}$$

$$\rho_m \frac{\partial \nu_x}{\partial t} = \frac{\partial \tau_{xy}}{\partial y} \tag{16}$$

where τ_{yz} and τ_{xy} are the shear stress, and ρ_m is the density of polymer melt.

From the inspection of eqs. (15) and (16), we can come to the conclusion that under the impact of the vibration field, the shear stress is a function regarding t and y, which is different from conventional extruders. Herein, the Tanner model constitutive equation is used for present analysis.

$$\tau_{zy} + \lambda \frac{\partial \tau_{zy}}{\partial t} = \eta(\dot{\gamma}) \frac{\partial \nu_z}{\partial y} \tag{17}$$

$$\tau_{xy} + \lambda \frac{\partial \tau_{xy}}{\partial t} = \eta(\dot{\gamma}) \frac{\partial \nu_x}{\partial y} \tag{18}$$

$$\eta(\dot{\gamma}) = K\left[\left(\frac{d\nu_x}{dy}\right)^2 + \left(\frac{d\nu_z}{dy}\right)^2\right]^{n-1/2} \tag{19}$$

Where λ denotes the relaxation time of polymer, K denotes the dense coefficient of polymer, and n denotes the power law index. In the present analysis, since we mainly take the effect of vibration field imposed on the flow field into consideration, the issues of space distribution of the flowing-field appears relatively less important. To facilitate the calculation, the average nominal shear rate is used to approximately solve the above equations, and we can get

$$\tau_{zy} + \lambda \frac{\partial \tau_{zy}}{\partial t} = \bar{\eta} \frac{\partial \nu_z}{\partial y} \tag{20}$$

$$\tau_{xy} + \lambda \frac{\partial \tau_{xy}}{\partial t} = \bar{\eta} \frac{\partial \nu_x}{\partial y} \tag{21}$$

$$\bar{\eta} = K\left[\frac{(\bar{V}_x^2 + \bar{V}_z^2)^{\frac{n-1}{2}}}{\bar{\delta}^{n-1}}\right] \tag{22}$$

where $\bar{\delta}$ is the mean thickness of melt film, $\bar{V}_x$ and $\bar{V}_z$ can be obtained from the following deduction:

We can assume that the melt is flowing along a certain direction in the double-plate model, which is similar to that shown in Figure 5. The apparent viscosity is η, the nominal shear rate is $\frac{V}{\bar{\delta}}$, then the viscosity dissipation heat per unit time is $dW = \eta\left(\frac{V}{\bar{\delta}}\right)^2 dt$, which is assumed to be equal to that generated by Newton liquid flowing in the same model, with shear rate $\frac{\bar{V}}{\bar{\delta}}$, that is

$$W = \frac{1}{T}\int_0^T \eta\left(\frac{V}{\bar{\delta}}\right)^2 dt = \eta\left(\frac{\bar{V}}{\bar{\delta}}\right)^2 \tag{23}$$

So, we obtain (for details see Appendix)

$$\bar{V}_x = \left(V_b^2 \sin^2\theta + \frac{1}{2}A^2\omega^2\cos^2\theta \right)^{\frac{1}{2}} \quad (24)$$

$$\bar{V}_z = \left[(V_b\cos\theta - V_{sz})^2 + \frac{1}{2}A^2\omega^2\sin^2\theta \right]^{\frac{1}{2}} \quad (25)$$

Then by solving eqs. (15), (16), (20), and (21), we obtain

$$\rho_m \frac{\partial \nu_z}{\partial t} + \lambda\rho_m \frac{\partial^2 \nu_z}{\partial t^2} - \bar{\eta}\frac{\partial^2 \nu_z}{\partial y^2} = 0 \quad (26)$$

$$\rho_m \frac{\partial \nu_x}{\partial t} + \lambda\rho_m \frac{\partial^2 \nu_x}{\partial t^2} - \bar{\eta}\frac{\partial^2 \nu_x}{\partial y^2} = 0 \quad (27)$$

With the boundary conditions

$$\begin{cases} y = 0 & \nu_x = 0 & \nu_z = 0 \\ y = \delta & \nu_x = V_x & \nu_z = V_z \end{cases} \quad (28)$$

and initial conditions

$$\begin{cases} t = 0 & \nu_x = 0 & \nu_z = 0 \\ t = 0 & \dfrac{d\nu_x}{dt} = 0 & \dfrac{d\nu_z}{dt} = 0 \end{cases} \quad (29)$$

Then, considering the boundary and initial conditions and solving eqs. (26) and (27), we obtain

$$\nu_x = k_2(k_5 y + k_4 y^3 + k_3 y^5)\cos\theta\cos(\omega t)/\delta + V_{bx} y/\delta \quad (30)$$

$$\nu_z = k_2(k_5 y + k_4 y^3 + k_3 y^5)\sin\theta\cos(\omega t)/\delta + (V_{bz} - V_{sz})y/\delta \quad (31)$$

where

$$k_2 = \frac{36A\omega}{(6 - \omega^2\rho_m\lambda\bar{\delta}^2/\bar{\eta})^2 + \omega^2\rho_m^2\bar{\delta}^4/\bar{\eta}^2} \quad (32)$$

$$k_3 = [\omega^4\rho_m^4\bar{\delta}^4(1 + 2\lambda^2\omega^2 + \lambda^4\omega^4)/\bar{\eta}^4 + 36\omega^2\rho_m^2 \times (1 + \omega^2\lambda^2)/\bar{\eta}^2 - 12\omega^4\rho_m^3\bar{\delta}^2\lambda \times (1 + \lambda^2\omega^2)/\bar{\eta}^3]/2592 \quad (33)$$

$$k_4 = [144\omega^4\rho_m^2\lambda^2\bar{\delta}^2/\bar{\eta}^2 - 12\omega^4\rho_m^3\bar{\delta}^4\lambda \times (1 + \lambda^2\omega^2)/\bar{\eta}^3 - 432\omega^2\rho_m\lambda/\bar{\eta}]/2592 \quad (34)$$

Then combining eqs. (20), (21), (30), and (31), we obtain

$$\tau_{xy} = \frac{k_1}{\lambda}\{k_2(k_5 + 3k_4y^2 + 5k_3y^4)\sin\theta(\lambda\cos\omega t + \omega\lambda^2)(1 + \omega^2\lambda^2)\delta + \frac{\lambda(V_{bz} - V_{sz})}{\delta} + c_5\exp\left(\frac{-t}{\lambda}\right) \quad (35)$$

$$\tau_{xy} = \frac{k_1}{\lambda}\left\{\frac{k_2(k_5 + 3k_4y^2 + 5k_3y^4)\cos\theta(\lambda\cos\omega t + \omega\lambda^2)}{(1 + \omega^2\lambda^2)\delta} + \frac{\lambda V_{bx}}{\delta} + c_6\exp\left(\frac{-t}{\lambda}\right)\right\} \quad (36)$$

As mentioned previously, the heat conduction along y direction is the only way for energy conduction, and so the energy equation obtained us given as

$$k_m\frac{d^2T}{dy^2} + \tau_{yz}\left(\frac{d\nu_z}{dy}\right) + \tau_{xy}\left(\frac{d\nu_x}{dy}\right) = 0 \quad (37)$$

Substituting eqs. (30), (31), (35), and (36) into eq. (37) yields

$$k_m\frac{\mathrm{d}^2\mathrm{T}}{\mathrm{dy}^2} + \frac{\bar{\eta}}{\delta^2}\{\mathrm{k}_2^2(\mathrm{k}_5 + 3\mathrm{k}_4\mathrm{y}^2 + 5\mathrm{k}_3\mathrm{y}^4)^2(\cos^2\omega t + \omega\lambda\cos\omega t)(1 + \omega^2\lambda^2) + V_{bx}^2 + (V_{bz} - V_{sz})^2 + [V_{bx}\cos\theta + (V_{bz} - V_{sz})\sin\theta]k_2(k_5 + 3k_4y^2 + 5k_3y^4)\frac{\cos\omega t + (\cos\omega t + \omega\lambda)}{1 + \omega^2\lambda^2} = 0 \quad (38)$$

With the boundary conditions,

$$T(0) = T_m\, T(\delta) = T_b \quad (39)$$

Then at the solid–melt interface, the temperature gradient is

$$\left(\frac{dT}{dy}\right)_{y=0} = \frac{T_b - T_m}{\delta} + \frac{\bar{\eta}}{2k_m\delta}\left\{k_2^2\left[k_5^2 + k_4k_5\delta^2 + \frac{(9k_4^2 + 10k_3k_5)\delta^4}{15} + 15k_3k_4\delta^6 + 5k_3^2\delta^6/36\right]\frac{\cos^2\omega t + \omega\lambda\cos\omega t}{1 + \omega^2\lambda^2} + V_{bx}^2 + (V_{bx} - V_{sz})^2 + [V_{bz}\cos\theta + (V_{bc} - V_{sz})\sin\theta]k_2 \times (k_5 + k_4\delta^2/2 + k_3\delta^4/6)\frac{\cos\omega t + (\cos\omega t + \omega\lambda)}{1 + \omega^2\lambda^2}\right\} \quad (40)$$

Let

$$U_1 = \frac{\bar{\eta}}{2}\Bigg\{k_2^2\Bigg[k_5^2 + k_4k_5\bar{\delta}^2 + \frac{(9k_4^2 + 10k_3k_5)\bar{\delta}^4}{15} + 15k_3k_4\bar{\delta}^6 + 5k_3^2\bar{\delta}^8/36\Bigg]\frac{\cos^2\omega t + \omega\lambda\cos\omega t}{(1+\omega^2\lambda^2)} + V_{bx}^2 + (V_{bz} - V_{sz})^2 + [V_{bx}\cos\theta + (V_{bc} - V_{sz})\sin\theta]k_2 \times (k_5 + k_4\bar{\delta}^2/2 + k_3\bar{\delta}^4/6)\frac{\cos\omega t + (\cos\omega t + \omega\lambda)}{1+\omega^2\lambda^2}\Bigg\} \quad (41)$$

Hence, the heat conducted from melt film into the melt–solid interface can be obtained as

$$-[q_{my}]_{y=0} = \frac{k_m(T_b - T_m)}{\delta} + \frac{U_1}{\delta} \quad (42)$$

Analytical expression of the heat conducted out of the melt–solid interface into the solid bed

Assuming that no significant internal deformations occur in the solid bed, the heat transfer pattern is considered to result from conduction fluxing in y direction. Therefore, the energy equation of solid bed is obtained as

$$\rho_s c_s V_{sy}\frac{dT}{dy} = k_s\frac{d^2T}{dy^2} \quad (43)$$

With the boundary conditions,

$$\begin{array}{ll} y = 0 & T = T_m \\ y = -\infty & T = T_s \end{array} \quad (44)$$

where cs is the specific heat of polymer solid, and Ts is the temperature of solid bed. Then, by solving eq. (43), we obtain

$$\frac{T - T_S}{T_m - T_s} = \exp\left(\frac{V_{sy}}{\alpha_s}y\right) \quad (45)$$

Herein, $\alpha_s = \dfrac{k_s}{\rho_s c_s}$ is the thermal diffusivity coefficient of polymer, and the heat conducted out of the melt–solid interface into the solid bed is obtained.

$$-[q_{sy}]_{y=0} = k_s\left(\frac{dT}{dy}\right)_{y=0} = \rho_s c_s V_{sy}(T_m - T_s) \quad (46)$$

The thickness of melt film and the melting rate ψ

Substituting eqs. (42) and (46) into eq. (14) leads to

$$\frac{k_m(T_b - T_m)}{\delta} + \frac{U_1}{\delta} - \rho_s c_s V_{sy}(T_m - T_s) = V_{sy}\rho_s\lambda_0 \quad (47)$$

Then,

$$V_{sy} = \frac{k_m(T_b - T_m) + U_1}{\delta\rho_s[c_s(T_m - T_s) + \lambda_0]} \quad (48)$$

Before calculating the melting rate ψ, we must know the flowing rate qx. So, from the melt mechanism discussed previously, qx is given as

$$q_x = \int_0^\delta \nu_x\, dy \quad (49)$$

Then, substituting eq. (30) into eq. (49) yields

$$q_x = \int_0^\delta \{k_2(k_5y + k_4y^3 + k_3y^5)\cos\theta\cos(\omega t)/\delta + V_{bx}y/\delta\}\, dy \quad (50)$$

Solving eq. (50), we obtain

$$q_x = \delta U_2 \quad (51)$$

where,

$$U_2 = [k_2(k_5 + k_4\bar{\delta}^2/2 + k_3\bar{\delta}^4/3)\cos\theta\cos(\omega t) + V_{bx}]/2 \quad (52)$$

Solving eqs. (11), (48), (51), and (52), the thickness of melt film δ and the melting rate ψ can be expressed by the following equations.

$$\delta = \left\{\frac{k_m(T_b - T_m) + U_1}{\rho_m U_2[c_s(T_m - T_s) + \lambda_0]}X\right\}^{\frac{1}{2}} \quad (53)$$

$$\psi = \left\{\frac{\rho_m U_2[k_m(T_b - T_m) + U_1]}{[c_s(T_m - T_s) + \lambda_0]}\right\}^{\frac{1}{2}}X^{\frac{1}{2}} \quad (54)$$

From eqs. (41) and (52), we can know that, U_1 and U_2 are functions with relating to time, amplitude, and frequency. Therefore, the melting rate ψ and the thickness of melt film δ are time-dependent and are under the effect of vibration parameters (amplitude and frequency).

The average melting rate and melt film

As discussed above, the melting rate is time-dependent; hence, for obtaining a better solid bed distribution and a better melting capability of VISS extruder, finding the average melting rate becomes essential.

As the screw is vibrating along axis direction, the solid bed will work as a "unilateral direction valve." That is, when screw moves towards the die head, the polymer melt in the melt film will be dragged into the melt pool by the inner wall of the barrel. On the contrary, when the screw moves in the opposite direction, the solid bed will move towards the inner wall of the barrel under the impact of the pressure generated by the growth of melt pool, which holds back the melt in the melt pool into the melt film. So, from eq. (49) we can get

$$\bar{q}_x = \left[\frac{\omega}{2\pi}\int_0^{\frac{2\pi}{\omega}} (q_x)^2\, dt\right]^{\frac{1}{2}} = \delta \bar{U}_2 \tag{55}$$

where,

$$\bar{U}_2 = \{[k_2^2(k_5 + k_4\bar{\delta}^2/2 + k_3\bar{\delta}^4/3)^2 \cos^2\theta + 2V_{bx}^2]/8\}^{\frac{1}{2}} \tag{56}$$

For the same reason, from eq. (42) we obtain

$$-\overline{[q_{my}]}_{y=0} = -\frac{\omega}{2\pi}\int_0^{\frac{2\pi}{\omega}} \overline{[q_{my}]}_{y=0}\, dt = \frac{k_m(T_b - T_m)}{\delta} + \frac{\bar{\eta}_1 \bar{U}_1}{\delta} \tag{57}$$

where,

$$\bar{U}_1 = \frac{\bar{\eta}}{2}\left\{k_2^2[k_5^2 + k_4k_5\bar{\delta}^2 + (9k_4^2 + 10k_3k_5)\bar{\delta}^4/15 + 15k_3k_4\bar{\delta}^6 + 5k_3^2\bar{\delta}^8/36]/(2 + 2\omega^2\lambda^2) + V_{bx}^2 + (V_{bz} - V_{sz})^2 + [V_{bx}\cos\theta + (V_{bz} - V_{sz})\sin\theta]\frac{k_2(k_5 + k_4\bar{\delta}^2/2 + k_3\bar{\delta}^4/6)\omega\lambda}{1 + \omega^2\lambda^2}\right\} \tag{58}$$

So, the mean melt film and melting rate obtained are as follows:

$$\bar{\delta} = \left\{\frac{k_m(T_b - T_m) + \bar{U}_1}{\rho_m \bar{U}_2[c_s(T_m - T_s) + \lambda_0]}X\right\}^{\frac{1}{2}} \tag{59}$$

$$\bar{\psi} = \phi X^{\frac{1}{2}} \tag{60}$$

where,

$$\phi = \left\{\frac{\rho_m \bar{U}_2[k_m(T_b - T_m) + \bar{U}_1]}{[c_s(T_m - T_s) + \lambda_0]}\right\}^{\frac{1}{2}} \tag{61}$$

THE SOLID BED DISTRIBUTION AND THE MELTING LENGTH

Tapered screw

Herein, the depth of screw channel H diminishes linearly over the melting section from an initial value H1 to a final value H3. The starting point of melting section is at z = 0, where the width of solid bed is X = W, and W is the width of screw channel, and so the channel depth is

$$H = H_1 - \alpha z \tag{62}$$

where H1 is the depth of screw channel at z = 0, and α is the pitch. Making the first order difference of eq. (62) we obtain

$$dH = -\alpha\, dz \tag{63}$$

Right and left hand sides of eq. (63) divided by d(HX) synchronously yields

$$\frac{d(HX)}{dH} = -\frac{d(HX)}{\alpha dz} \tag{64}$$

Substituting eq. (64) into eq. (10), and assuming that the effect of the vibration field on the movement of solid bed can be neglected, we obtain

$$-\alpha\frac{d(HX)}{dH} = -\frac{\bar{\psi}}{\rho_s V_{sz}} \tag{65}$$

From eq. (60), eq. (65) can be simplified as

$$\frac{d(HX)}{dH} = \frac{\phi X^{\frac{1}{2}}}{\alpha\rho_s V_{sz}} \tag{66}$$

or

$$X + H\frac{dX}{dH} = \frac{\phi X^{\frac{1}{2}}}{\alpha\rho_s V_{sz}} \tag{67}$$

Considering the boundary conditions,

$$z = Z_0\ X = X_0 \tag{68}$$

Equation (67) can be solved as

$$X = \left[\frac{\phi}{\alpha\rho_s V_{sz}} + \left(\frac{-\phi}{\alpha\rho_s V_{sz}} + X_0^{\frac{1}{2}}\right)\left(\frac{H_1 - \alpha Z_0}{H_1 - \alpha z}\right)^{\frac{1}{2}}\right]^2 \quad (69)$$

When X = 0, the melted material fills the entire cross section of the screw channel, and the solid bed disappears. Therefore, the length of mix-melting section ZT is obtained as

$$Z_T = \frac{H_1 - \left(1 - \frac{\alpha\rho_s V_{sz} X_0^{\frac{1}{2}}}{\phi}\right)^2 (H_1 - \alpha Z_0)}{\alpha} \quad (70)$$

From eq. (70), we know that when ϕ is large enough, $\frac{\alpha\rho_s V_{sz} W_1^{\frac{1}{2}}}{\phi} < 1$, and hence, Z_T decreases as the ϕ increases. Furthermore, as expressed in eq. (61), ϕ is a function relating to parameters of vibration field, and so Z_T is also relative to the vibration parameters.

Nontapered screw

Under this condition, the depth of screw channel H is constant in z direction; therefore, from eq. (10) we obtain

$$\frac{dX}{dZ} = -\frac{\bar{\psi}}{H\rho_s V_{sz}} = -\frac{\phi X^{\frac{1}{2}}}{H\rho_s V_{sz}} \quad (71)$$

Considering the boundary conditions,

$$z = Z_1 \; X = X_1 \quad (72)$$

Then, by solving eq. (71), we obtain

$$X = X_1\left(1 - \frac{\phi(z - Z_1)}{2HV_{sz}\rho_s X_1^{\frac{1}{2}}}\right)^2 \quad (73)$$

As mentioned earlier, when X = 0, the solid bed will disappear, and hence, the melting section length Z_T' is

$$Z_T' = Z_1 + \frac{2HV_{sz}\rho_s X_1^{\frac{1}{2}}}{\phi} \quad (74)$$

Inspection of eqs. (70) and (74) reveals that the melting section length is relative to the rotation speed of screw, the temperature of barrel, the amplitude and frequency of vibration, and the physical and rheologic performance of material. Of course, in the present analysis, we will focus on the amplitude and frequency of vibration.

POWER CONSUMPTION IN MELTING SECTION

As stated earlier, the melting section is filled both by polymer solid and melt, and so it is difficult to analyze the power consumption precisely. Herein, to simplify the calculation, we assume that the energy of melting section is mostly consumed at the inner wall of barrel, where $y = \bar{\delta}$, and so from eqs. (35) and (36), we have

$$P_z = \tau_{zy} V_z = k_1 WZ \left\{\frac{k_2(k_5 + 3k_4\bar{\delta}^2 + 5k_3\bar{\delta}^4)\sin\theta(\cos\omega t + \omega\lambda)}{(1 + \omega^2\lambda^2)\bar{\delta}} + \frac{(V_{bz} - V_{sz})}{\delta}\right\}(V_{bz} - V_{sz} + A\omega\sin\theta\cos\omega t) \quad (75)$$

$$P_x = \tau_{xy} V_x = k_1 WZ \left\{\frac{k_2(k_5 + 3k_4\bar{\delta}^2 + 5k_3\bar{\delta}^4)\cos\theta(\cos\omega t + \omega\lambda)}{(1 + \omega^2\lambda^2)\bar{\delta}} + \frac{V_{bx}}{\delta}\right\}(V_{bx} + A\omega\cos\theta\cos\omega t) \quad (76)$$

where P_z and P_x is the power consumption of melting section along z and x direction, respectively; Z is the length of melting section. Then, the total power consumption of melting section can be obtained as

$$P = P_z + P_x \quad (77)$$

From previous equations, we can know that the total power consumption of melting section is a function of time, and so the mean power consumption can be solved:

$$\bar{P} = \frac{\omega}{2\pi}\int_0^{\frac{2\pi}{\omega}} P dt = \frac{k_1 WZ}{\bar{\delta}}\left\{k_2(k_5 + 3k_4\bar{\delta}^2 + 5k_3\bar{\delta}^4)\frac{A\omega/2 + V_{bx}\omega\lambda\cos\theta + (V_{bz} - V_{sz})\omega\lambda\sin\theta}{1 + \omega^2\lambda^2} + [V_{bx}^2 + (V_{bz} - V_{sz})^2]\right\} \quad (78)$$

Then from eqs. (70), (74), and (78), we have the following equation when the screw is tapered

$$\bar{P}_1 = \frac{\bar{\eta}W}{\bar{\delta}}\left\{k_2(k_5 + 3k_4\bar{\delta}^2 + 5k_3\bar{\delta}^4)\frac{A\omega/2 + V_{bx}\omega\lambda\cos\theta + (V_{bz} - V_{sz})\omega\lambda\sin\theta}{1 + \omega^2\lambda^2} + [V_{bx}^2 + (V_{bz} - V_{sz})^2]\right\}\frac{H_1 - (1 - \alpha\rho_s V_{sz} X_0^{\frac{1}{2}}/\varphi)^2(H_1 - \alpha Z_0)}{\alpha} \quad (79)$$

TABLE I
Parameter of Screw

D (mm)	θ	H_1 (mm)	H_3 (mm)	L (mm)	W (mm)	E (mm)
20	17.65°	3.2	1.1	120	17	2

when the screw is nontapered,

$$\bar{P}_2 = \frac{\bar{\eta}W}{\bar{\delta}}\left\{k_2(k_5 + 3k_4\bar{\delta}^2 + 5k_3\bar{\delta}^4)\right.$$
$$\frac{A\omega/2 + V_{bx}\omega\lambda\cos\theta + (V_{bz} - V_{sz})\omega\lambda\sin\theta}{1 + \omega^2\lambda^2}$$
$$\left. + [V_{bx}^2 + (V_{bz} - V_{sz})^2]\right\}\frac{Z_1 + 2HV_{sz}\rho_s X_1^{\bar{2}}}{\phi}^{1} \quad (80)$$

EXPERIMENT AND CALCULATION SAMPLE

Equipment

The H-VISS extruder together with the measurement and date gathering system were used in the present experiment. It was made in the National Engineering Research Center of Novel Equipment for Polymer Processing, South China University of Technology. As shown in Figure 1, the screw of this apparatus can vibrate along its axis direction as it rotates. The vibration frequency can be up to the maximum value 40 Hz, and the maximum amplitude is 2 mm. Parameters of the screw are given in Table I. Where D is the diameter of the screw, θ is the helix angle, H_1 is the channel depth of the feed section of the screw, H_3 is the channel depth of the metering section of the screw, L is the length of compression in axis direction, W is the width of screw channel, and e is the width of screw flight.

Materials

LDPE (951–050, made in petrochemicals Co. Ltd. Maoming of china) was used in the present experiment and theoretical calculation, and the physical performance of this is given in Tables II and III, and the power law constants are $K = 5.6 \times 10^4$, $n = 0.335$, $\lambda = 1.5$, and $\bar{\delta} = 0.02$ (for other calculations)

TABLE II
Physical Properties of Solid LDPE (951–050)

ρ_s (kg/m^3)	T_g (°C)	k_s (W/m °C)	C_{ps} (KJ/Kg °C)	λ (KJ/Kg)
915	−68	0.335	2.76	129.8

TABLE III
Physical Properties of LDPE (951–050) Melt

ρ_m (Kg/m^3)	T_m (°C)	k_m (W/m °C)	C_m (KJ/Kg °C)
810	110	0.24	2.43

Experimental procedure

To the H-VISS extruder experiment, the temperature of the compression section, the melt conveying section, and the die were set at 140, 180, and 170°C, respectively. After temperature arrives at the set value, the electromotor (supply for the screw rotation) and the oscillator (supply for the screw vibration) starts working. The rotation speed of the screw is controlled at 60 rpm. Adjust the frequency of vibration from 0 to 25 Hz (the space is 5 Hz), and the amplitude from 0 to 0.8 mm (the space is 0.2 mm). At each step, after the H-VISS extruder is running in steady condition at a certain combination of vibration parameters for about 3 min, quickly stop the electromotor and the oscillator followed by rapid cooling of the barrel, then open the barrel and get the material ribbons labeled with numbers (shown in Fig. 2). Afterwards, close the barrel and the next step of experiment with other vibration parameters is performed. Finally, the material ribbons removed from the screw are cross-sectioned in various places and the material slices are derived as shown in Figure 3. Through measuring the geometric size of these slices, the polymer solid bed distribution and melting length are obtained.

RESULTS AND DISCUSSION

In the classical melting theory,[8–21] the melting section length, the melting rate, and the solid bed distribution are the three main factors for extruder's melting capacity. That is, the shorter the melting length (or the rapider decrease of the solid bed in z direction) and the quicker the melting rate, the higher the melting capacity of extruder. As mentioned earlier, in the present experiment, the barrel of H-VISS extruder can be opened (shows in Fig. 1). Therefore, the melting section length and the solid bed distribution can be obtained from the direct measurement of the material slice (see Figs. 2 and 3). Yet, it is difficult to get the data of melting rate and power consumption from the present experiment. Hence, in the following results, the melting rate, the melt film thickness, and the power consumption have no experimental results. Fortunately with the help of the results of melting section length and solid bed distribution, the previous theory (physical model and analytical expressions) can be proved efficiently.

The introduction of vibration force field can accelerate the disentwining-tangle speed of polymer hu-

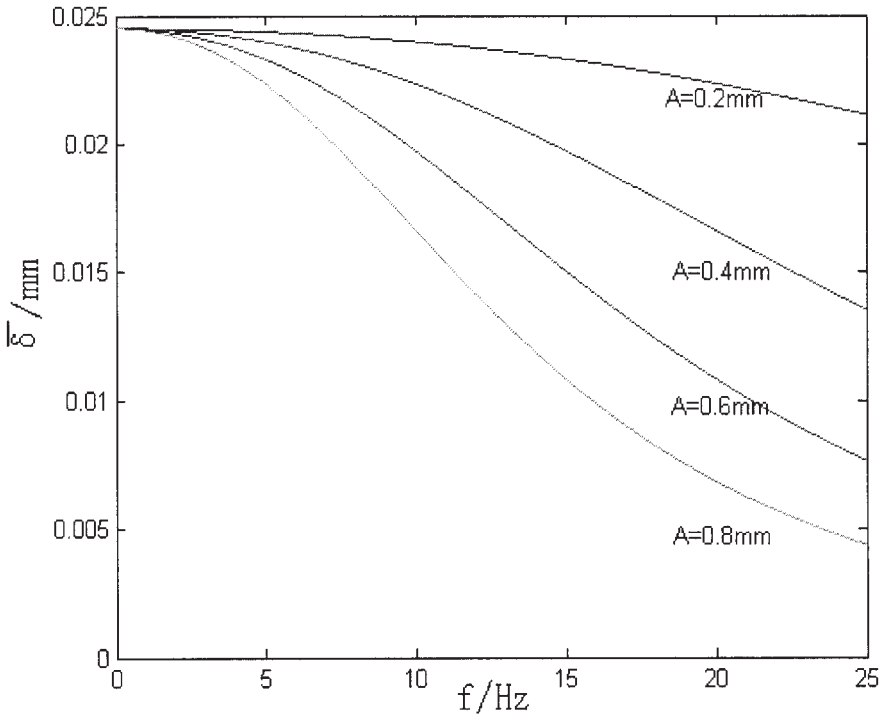

Figure 6 Relationship between the average thickness and the vibration parameters obtained from theoretical calculation (A is the vibration amplitude and f is the vibration frequency).

man molecule, decrease the viscoelasticity of polymer melt, and both of which will lead to lessening the resistance to melt's flowing. Therefore, polymer melt can be trailed into the melt pool easily. Simultaneously, as stated earlier, under the impact of vibration force field, the solid bed will work as a "unilateral direction valve." Thereby, the thickness of the melt film will decrease as the vibration parameters increase (shows in Fig. 6). As it is well known, when the shear velocity is constant, the more thin the melt film, the higher the shear rate is. So from energy equation, we can know that the viscidity dissipation will increase rapidly as vibration parameters increase. Furthermore, with the decrease of melt film thickness, the heat conducted out of the barrel into the solid bed becomes very easy. Accordingly, with the increase of the vibration amplitude and frequency, the average melting rate will increase (as shown in Fig. 7), the average power consumption and the melting section length will decrease (see in Figs. 8 and 9), and the curve of the solid bed distribution in z direction will descend more and more rapidly (see in Fig. 10).

The average melting rates under various vibration amplitudes (at $X = 10$ mm, X is the width of solid bed) are shown as a function of vibration frequency in Figure 7. Where $\bar{\psi}$ is the average melting rate, and A and f are the vibration amplitude and frequency, respectively. It is clear that the average melting rate is lowest right at the initiatory stage of the curve ($f < 5$ Hz) and highest at the end ($f = 25$), and the average melting rate increases as the vibration amplitude and frequency increases. As shown in Figure 7, the intersection ($f = 0$) between the curve and the ordinate is the melting rate of conventional extruder (without vibration force field). This particularly becomes apparent from Figure 7, where $\bar{\psi}$ is about 0.0019 kg/(m s) at $f = 0$ Hz and 0.0039 kg/(m s) at $f = 25$ Hz and $A = 0.8$ mm (a 105.3% increase relative to $f = 0$).

The melting section lengths Z_T are plotted in Figure 8 as a function of vibration parameters. As shown in Figure 8, there are four curves representing the relationship between Z_T and f of each of the amplitudes ($A = 0.2$, 0.4, 0.6, and 0.8 mm, respectively). When $A = 0.8$ mm, the Z_T is found to be decreased from about 555 to about 345 mm (a 37.9% decrease), going from $f = 0$ to $f = 25$ Hz. Similarly, the Z_T decreases from about 555 to about 380, 430, and 500 mm under the conditions that $A = 0.6$ mm, $A = 0.4$ mm, and $A = 0.2$ mm, respectively. This clearly indicates that the melting section length of VISS extruder decreases as the vibration parameters increases.

Figure 9 shows the average power consumption ($\bar{P}$) in melting section decreases as the vibration parameters increase. As seen in Figure 9, when $A = 0.8$ mm, the average power consumptions decrease from about 85 to about 20 W in traversing from $f = 0$ Hz to $f = 25$ Hz (a about 70.5% decrease), and as mentioned earlier, when $f = 0$ Hz, the intersection between the curve and the ordinate is the power consumption of conven-

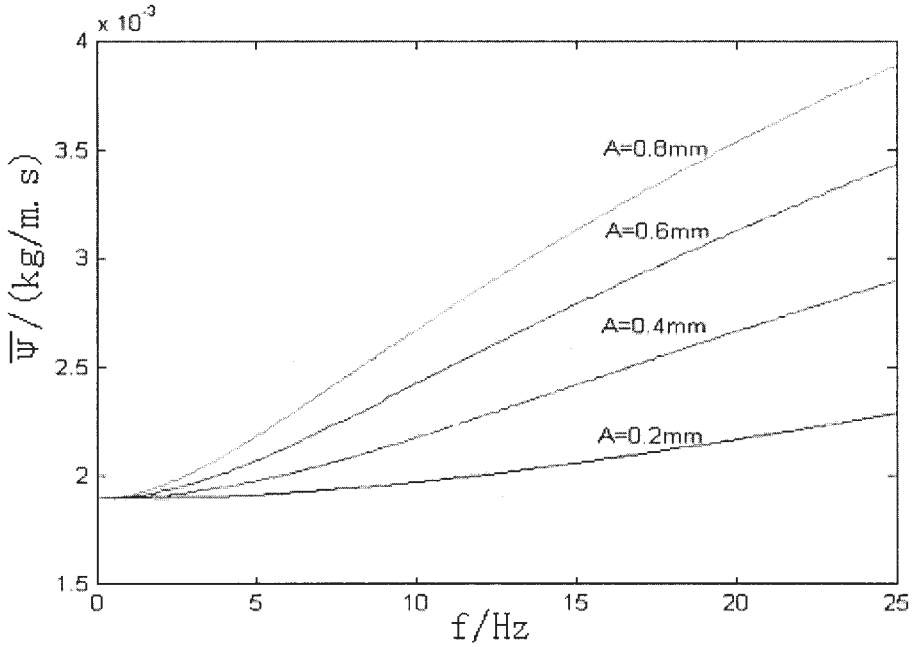

Figure 7 Relationship between the average melting rate and the vibration parameters obtained from theoretical calculation at $X = 10$ mm.

tional extruder (without vibration field). Similarly, when $f = 25$ Hz, the power consumptions decrease from 50 to about 20 W, going from $A = 0.2$ mm to $A = 0.8$ mm (a 60% decrease). Combining all of the aforementioned data, it appears that the introduction of vibration force field can economize power consumption to a great degree. Inspecting the curves plotted in Figure 9 reveals that when the intensity of

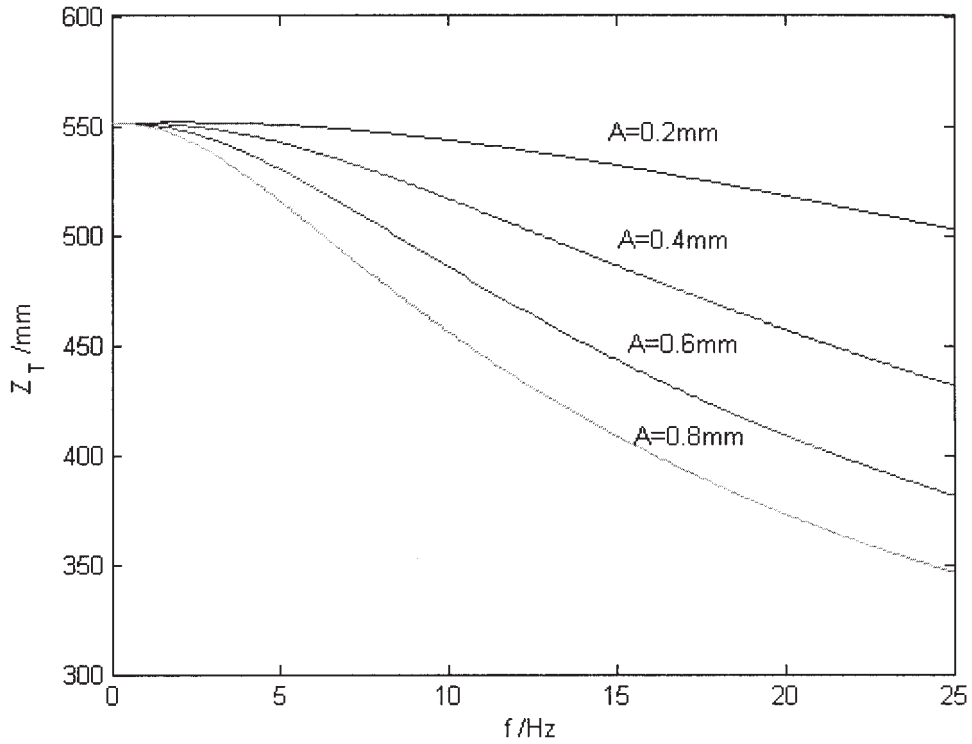

Figure 8 Relationship between the length of melting section (Z_T) and the vibration parameters obtained from theoretical calculation.

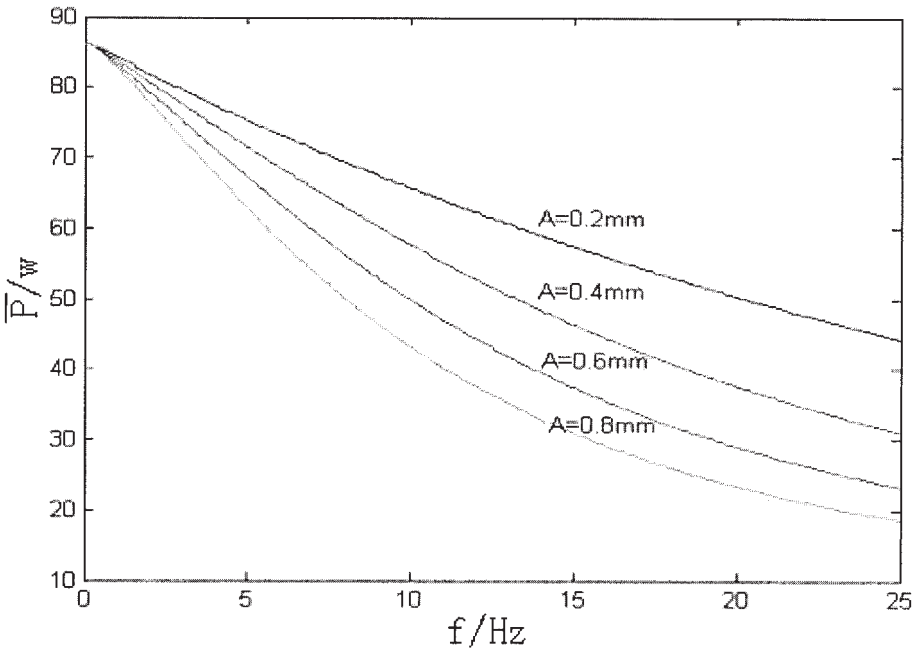

Figure 9 Relationship between the average power consumption and the vibration parameters obtained from calculation sample.

vibration arrives at an extremum, continuing to increase the vibration parameters did not lead to a significant change on the average power consumption, since it had already reached to a relative steady value. That is, the average power consumption can not be equal to zero, which is in agreement to the practical condition.

Figure 10 is the illustration of the relationship between the solid bed distribution and the vibration parameters coming from theoretic calculation. In

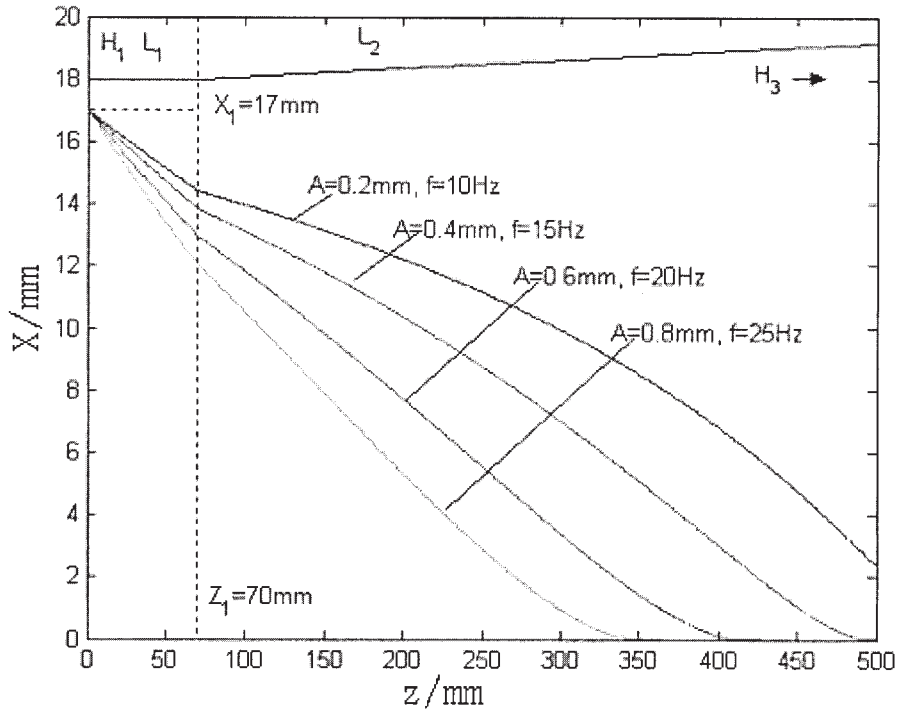

Figure 10 Relationship between the solid-bed distribution and the vibration parameters obtained from calculation sample.

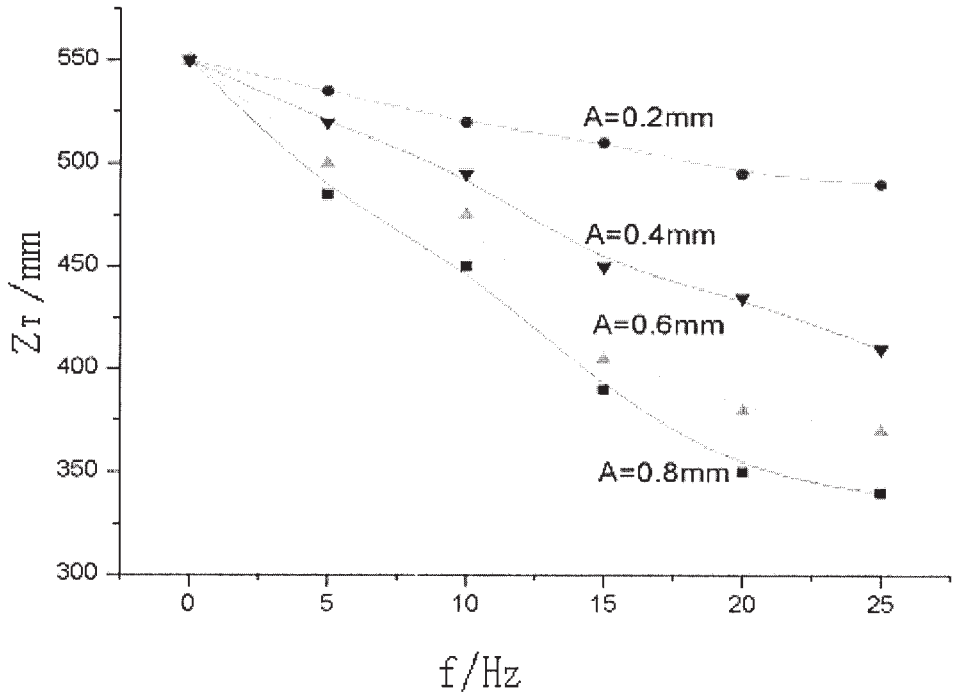

Figure 11 Relationship between the melting section length (Z_T) and the vibration parameters obtained from experiment.

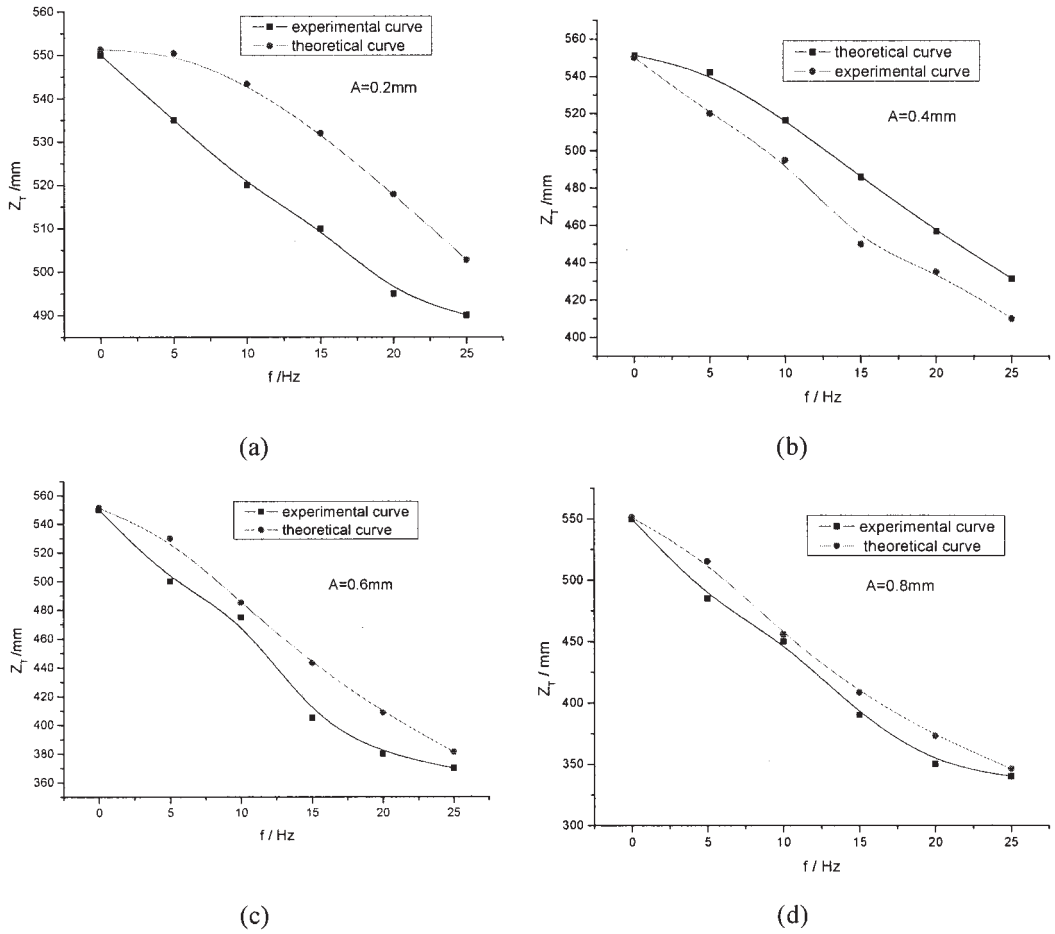

Figure 12 Comparison illustrations of the melting section length obtained from experimental and theoretical calculation (a) $A = 2$ mm, (b) $A = 0.4$ mm, (c) $A = 0.6$ mm, and (d) $A = 0.8$ mm.

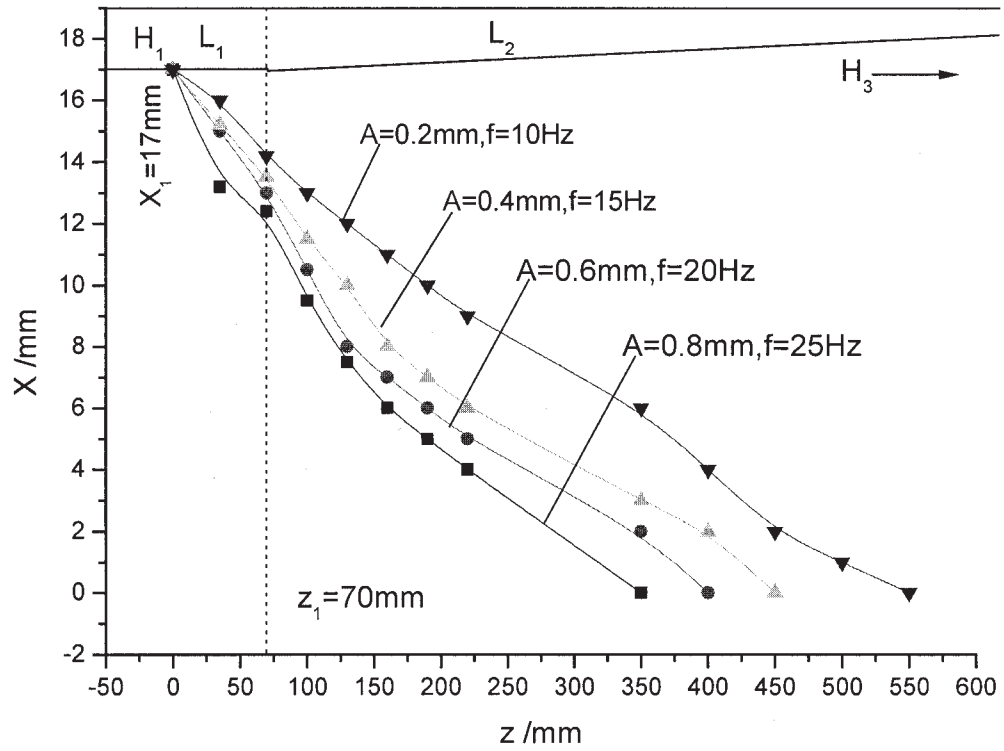

Figure l3 Relationship between the solid-bed distribution and the vibration parameters obtained from experiment.

Figure 10, we assume that $z = 0$ is the starting point of melting section, abscissa (z) is down screw channel direction, ordinate (X) is the width of solid bed, L_1 is the length of feed section, H_1 is the screw channel depth, L_2 is the length of compression section, and H_3 is the screw channel depth of metering section, respectively. As shown in Figure 10, when $Z \approx 70$ mm, there is a turning point in any of these four curves. This is because that the melting process occurs both on the feed section and compression section of the screw. The right hand to this point is the compression section and eq. (69) should be used, and the other side is the feed section and eq. (73) should be used. The declining rate of the curves plotted in Figure 10 decrease as the vibration parameters (A and f) increase, which indicates that the increase of the vibration parameters can better the melting capacity of extruder. As shown in Figure 10, when $X = 0$, the solid bed disappeared and the screw channel was filled by polymer melt entirely. So, the intersections of these curves and the abscissa are the length of melting section, which is consistent with Figure 8.

Figure 11 is the illustration of the relationship between the melting section length and the vibration parameters obtained from the experiment, while Figure 12 is the comparison illustrations of the melting section lengths coming from experiment and theoretical calculation (under various combination of vibration parameters). It is clearly seen in Figure 11 that the increase of vibration amplitude and frequency can shorten the length of the melting section, which is in good agreement with the calculated results. As seen in Figure 12, although those results of experiment are very well consistent with those of theoretical calculation , there are still minor deviations among them, especially in Figure 12(a). This is because, during the course of the theory deduction and to obtain the analytical expressions of the melting model, many assumptions are hold to be true, which can not be neglected in the indeed course of extrusion. On the other hand, test error is another reason for the deviation.

Figure 13 shows the course of melting along the screw channel in terms of the distribution of the solid bed. Same as what is shown in Figure 10, the abscissa z is along down screw channel direction, the ordinate X represents the width of the solid bed, $H_1 = 3.2$ mm and $H_3 = 1.1$ mm, and so on. In agreement with our theoretical calculations, the declining rate of these curves (distribution of the solid bed) decrease as the vibration amplitude and frequency increase. However, the turning point is unconspicuous in experimental results, which is resulted from the testing or measuring error. Figure 14 is the comparison illustration of the solid bed distribution coming from experimental and theoretical calculation (under various combination of vibration parameters). As shown in Figure 14, when $A = 0.2$ mm, $f = 10$ Hz, and $z = 70$ mm, the solid bed width

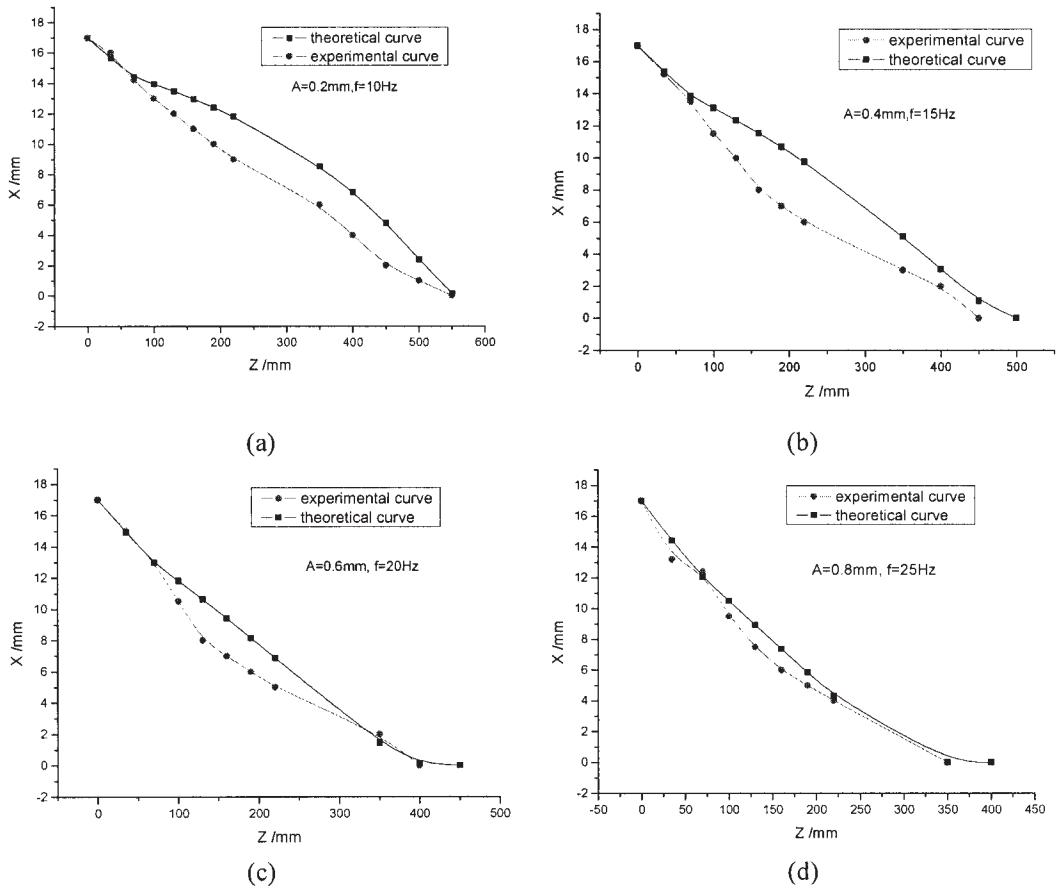

Figure l4 Comparison illustration of the solid-bed distribution obtained from experimental and theoretical calculation (a) A = 0.2 mm, f = 20 Hz; (b) A = 0.4 mm, f = l5 Hz; (c) A = 0.6 mm, f = 20 Hz; and (d) A = 0.8 mm, f = 25 Kz.

X that comes from experiment is equal to 14 mm (Fig. 12), and the X that come from theoretical calculation is equal to 14.4028 mm, and the deviation between the two data is only 0.4028 mm (a less than 3% error relative to experimental value). Figures 14(a)–14(d) have proved that the theoretical model presented here is accurate, efficient, and usable.

CONCLUSIONS

Through the H-VISS visualization experimental observation, the melting mechanism is researched deeply and the reliable physical model is established. Subsequently, the mathematical analytical model is derived by the sophisticated mathematical deduction. The key feature of the present model is as follows: The vibration force field is introduced into the whole course of the extrusion, then the velocity, the pressure, the temperature, and the viscidity in the polymer melt of VISS extruder behave strongly nonlinear and time-dependent, and the viscous dissipation become more important than that of conventional extruders. The melting rate, the melt film thickness, the melting section length, the power consumption, and the solid bed distribution of VISS extruder are captured in this model. Finally, it is proved by visualization experiment.

The comparison of the results coming from the theoretical calculation and the H-VISS experiment reveals that the introduction of the vibration force field into the whole course of the extrusion can improve the melting capacity and economize the power consumption of extruder greatly.

This study will serve as the theory basis for the optimum conditions of vibration extruder design and processing polymer.

APPENDIX

From the aforementioned deduction, we have

$$W = \frac{1}{T}\int_0^T \eta\left(\frac{V}{\bar{\delta}}\right)^2 dt = \eta\left(\frac{\bar{V}}{\bar{\delta}}\right)^2 \qquad (A.1)$$

$$V_x = V_{bx} + V_{dx} \qquad (A.2)$$

$$V_z = V_{bz} + V_{dz} - V_{sz} \quad (A.3)$$

$$V_{bx} = V_b \sin\theta \quad (A.4)$$

$$V_{bz} = V_b \cos\theta \quad (A.5)$$

$$V_{dz} = A\omega \sin\theta \cos\omega t \; V_{dx} = A\omega \cos\theta \cos\omega t \quad (A.6)$$

Substituting eqs. (A.4), (A.5), and (A.6) into eqs. (A.2) and (A.3), respectively, leads to

$$V_x = V_b \sin\theta + A\omega \cos\theta \cos\omega t \quad (A.7)$$

$$V_z = V_b \cos\theta + A\omega \sin\theta \cos\omega t - V_{sz} \quad (A.8)$$

Substituting eqs. (A.7) and (A.8) into eq. (A.1) leads to

$$\frac{1}{T}\int_0^T \eta\left(\frac{V_b \sin\theta + A\omega \cos\theta \cos\omega t}{\bar{\delta}}\right)^2 dt = \eta\left(\frac{\bar{V}_x}{\bar{\delta}}\right)^2 \quad (A.9)$$

$$\frac{1}{T}\int_0^T \eta\left(\frac{V_b \cos\theta + A\omega \sin\theta \cos\omega t - V_{sz}}{\bar{\delta}}\right)^2 dt = \eta\left(\frac{\bar{V}_z}{\bar{\delta}}\right)^2 \quad (A.10)$$

Solving eqs. (A.9) and (A.10), we obtain

$$\bar{V}_x = \left(V_b^2 \sin^2\theta + \frac{1}{2}A^2\omega^2 \cos^2\theta\right)^{\frac{1}{2}} \quad (A.11)$$

$$\bar{V}_z = \left[(V_b \cos\theta - V_{sz})^2 + \frac{1}{2}A^2\omega^2 \sin^2\theta\right]^{\frac{1}{2}} \quad (A.12)$$

References

1. Qu, J. P. Nat Sci 1992, 20, 1.
2. Qu, J. P. U.S. Pat. 5,217,302 (1993).
3. Feng, Y. H. Doctoral Thesis, South China University of Technology, Guangzhou, China, 2003.
4. Wu, H. W.; Zhou, N. Q.; He, H. Z.; Qu, J. P. China Plast 1996, 10, 53.
5. Peng, X. F.; Qu, J. P.; Li, L. F. Eng Plast Appl 1999, 27, 38.
6. Qu, J. P.; Qing, Y. M.; Tian, Y. C.; Zhou, N. Q. China Plast Ind 2000, 28, 23.
7. Qu, J. P.; Chen, X. F. Light Ind Mach 2004, 1, 21.
8. Tadmor, Z. Polym Eng Sci 1966, 6, 185.
9. Tadmore, Z.; Klein, I. Engineering Principles of Plasticating Extrusion; Krieger: Malbar, FL, 1970.
10. Maddock, B. H. SPE J 1959, 15, 383.
11. Street, L. F. Int Plast Eng 1961, 1, 289.
12. Vermeulen, J. R.; Scargo, P. G.; Beek, W. J. Chem Eng Sci 1971, 26, 1457.
13. Edmondosn, I. R.; Fenner R. T. Polymer 1975, 16, 49.
14. Dekker, J. Kunststoffe 1976, 66, 130.
15. Lindt, J. T. Polym Eng Sci 1976, 16, 284.
16. Lindt, J. T. Polym Eng Sci 1985, 25, 585.
17. Lindt, J. T. Polym Eng Sci 1981, 21, 1162.
18. Bravo, V. L.; Hrymak, A. N.; Wright, J. D. Polym Eng Sci 2004, 44, 779.
19. Yung, K. L.; Xu, Y.; Lau, K. H. Polymer 2002, 43, 2543.
20. Shapiro, J.; Pearson, J. R. A.; Trottmow, R. Polymer 1978, 19, 1199.
21. Chung, K. H.; Chung, C. Polym Eng Sci 1983, 23, 191.